Biomacromolecules

Article

Cite This: Biomacromolecules 2019, 20, 3283−3293

pubs.acs.org/Biomac

Development of Adhesive and Conductive Resilin-Based Hydrogels for Wearable Sensors

Xiao Hu,[†] Xiao-Xia Xia,[†] Sheng-Chen Huang, and Zhi-Gang Qian*

State Key Laboratory of Microbial Metabolism, Joint International Research Laboratory of Metabolic & Developmental Sciences, and School of Life Sciences and Biotechnology, Shanghai Jiao Tong University, 800 Dongchuan Road, Shanghai 200240, People's Republic of China

Supporting Information

ABSTRACT: Integrating multifunctionality such as stretchability, adhesiveness, and electroconductivity on a single protein hydrogel is highly desirable for various applications, and remains a challenge. Here we present the development of such multifunctional hydrogels based on resilin, a natural rubber-like material with remarkable extensibility and resilience. First, genetically engineered reslin-like proteins (RLPs) with varying molecular weight were biosynthesized to tune mechanical strength and stiffness of the cross-linked RLP hydrogels. Second, glycerol was incorporated into the hydrogels to endow adhesive properties. Next, a graphene−RLP conjugate was synthesized for cross-linking with the unmodified, pristine RLP to form an integrated network. The obtained hybrid hydrogel could be stretched to over four times of its original length, and self-adhered to diverse substrate surfaces due to its high adhesion strength of ∼24 kPa. Furthermore, the hybrid hydrogel showed high sensitivity, with a gauge factor of 3.4 at 200% strain, and was capable of real-time monitoring human activities such as finger bending, swallowing, and phonating. Due to these favorable attributes, the graphene/resilin hybrid hydrogel was a promising material for use in wearable sensors. In addition, the above material design and functionalization strategy may provide intriguing opportunities to generate innovative materials for broad applications.

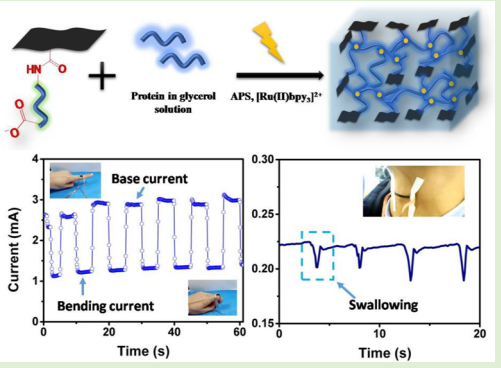

INTRODUCTION

Protein-based materials that are electrically conductive have recently emerged as promising substrates for applications such as flexible electronics, sensors, and actuators.[1,2] These applications require the conductive materials to be sensitive, stretchable, recoverable, and preferably adhesive to the complex surfaces of the human body. In particular, high stretchability and sensitivity to deformations are desirable for real-time monitoring of complex, full-range human motions such as finger bending, swallowing, and phonation.[3−5] Although many synthetic elastomers with desirable electromechanical properties have been rapidly developed, these nonprotein materials are not well suited for biological applications due to the lack of biodegradability. To overcome the limitation, protein-based materials with excellent performance need to be developed. Indeed, as a biobased and ecofriendly alternative to metal- and synthetic polymer-based counterparts, conductive protein-based materials have received an increasing amount of attention in recent years.[6,7]

Indeed, many attempts have been made to design and fabricate conductive materials from proteins that are naturally derived or recombinantly biosynthesized. One approach is to carbonize proteins into conductive graphitic nanocarbons directly by thermal treatment. For example, fabrics of cocoon silk were carbonized under an argon and hydrogen mixed atmosphere at temperatures up to 950 °C, and then made into strain sensors that were highly durable and sensitive, with a gauge factor (GF) of 9.6 for strain within 250%.[8] Although multiple features were desirably obtained, the silk carbonization process is energy intensive, and requires a special equipment for controlled heating. Another approach is to coat protein materials with conducting elements. In an early study, the natural *Nephila clavipes* dragline silk fibers were uniformly coated with amine-functionalized multiwalled carbon nanotubes.[9] The conductivity of the coated fibers was reversibly sensitive to strain with a GF of 1.2, yet their limited extensibility (a strain of 73%) and specificity (also humidity-sensitive)[9] might restrict the use as strain sensors. Alternatively, conductive materials can be made by integrating conductive elements into elastic networks of protein polymers. So far, nanomaterials such as metal nanowires[6] and low-dimentional carbons,[10−12] ionic carriers,[13] and ionic liquids[14] have been utilized as conductive elements due to their outstanding electrical properties. Recently, 3D printable graphene ink was dispersed in hexafluoroisopropanol or

Special Issue: ISBP2018

Received: March 19, 2019
Revised: April 23, 2019
Published: April 29, 2019

DOI: 10.1021/acs.biomac.9b00389
Biomacromolecules 2019, 20, 3283−3293

$CaCl_2$/formic acid solutions of silkworm silk and the resulting suspensions were processed into conductive polymorphic materials, such as films, fibers, and coating.[12] In particular, the silk/graphene composite film sensor had a linearly increased GF from 0.13 to 0.47 during deformation from 0% to 300%. However, the resistance of the film sensor could not be entirely recovered after large deformations, and thus the capability of cycle use was limited due to high hysteresis and permanent deformation of the films.[12] This problem is not uncommon for a majority of protein materials because the simply dispersed conductive elements are easily mobile within the protein materials under deformations and electric field. Thus, the development of conductive protein materials with both high sensitivity and stretchability remains a big challenge,[10−12] which is also true for the fabrication of synthetic polymer-based conductive materials.[15−19]

Resilin is one of the most extensible and resilient protein materials found in specialized regions of the cuticle of most insects.[20−22] To decode the genetic information on resilin, the fruitfly *Drosophila melanogaster* CG15920 gene was identified as a tentative one encoding a resilin-like protein (RLP).[20] Later, the first exon of the CG15920 gene was cloned and expressed in bacterium *Escherichia coli*,[21] and the recombinant RLP was photo-cross-linked into a rubber-like hydrogel biomaterial with resilience (>92%) and extensibility (~300%) comparable to that of natural resilin. Similar rubber-like properties were also observed in hydrogels fabricated from recombinant full-length resilin,[23] RLPs with only repetitive consensus motifs of resilin,[24,25] and even RLPs with re-engineered amino acid residues for cross-linking.[26−28] Due to the outstanding extensibility and elastic properties, the RLP hydrogels have shown great potential for applications in soft tissue engineering,[26−29] despite the relative low hydrogel strength and stiffness due to the intrinsically disordered feature of resilin.[22,23] To probe the molecular mechanism of resilin elasticity, the structure−function relationships have been explored.[30] In addition, many efforts have been devoted to characterize resilin,[23−25,31,32] and reveal its multiple stimuli responsiveness to several factors such as temperature, pH, and light, which has scarcely been reported for either synthetic or natural biopolymers.[31,33] The unique molecular flexibility and physical attributes of resilin indicate the great potential of resilin for the development of novel intelligent materials.[22,29,33]

We surmised that resilin might be a good starting matrix for functionalization into conductive materials with robust electro-mechanical properties desirable for use in wearable electronics. Therefore, this study aims to develop such resilin-based material, and to demonstrate its use in wearable sensors. First, we designed and biosynthesized a series of RLPs with varying numbers of the repetitive motifs to modulate hydrogel mechanical properties by varying the protein molecular weight (Mw). Next, glycerol was selected and added as a cosolvent into pregelation solutions of RLP to tune hydrogel mechanical properties further, and more importantly, impart adhesion properties to the hydrogels. Furthermore, graphene was conjugated to resilin for cross-linking with the unmodified, pristine resilin to form an integrated electroconductive matrix. The obtained hybrid hydrogel exhibited intriguing properties in combination, and demonstrated great potential as wearable sensors for real-time monitoring of both large-scale and tiny motions of human activities.

MATERIALS AND METHODS

Chemicals and Materials. Ampicillin, ethanol, glycerol (Catalog No. A100854), imidazole, and isopropyl-β-D-thiogalactopyranoside (IPTG) were obtained from Sangon Biotech (Shanghai, China). Dityrosine was purchased as a synthetic standard from WuXi AppTec Co., Ltd. (Shanghai, China). Graphene oxide (Catalog No. G0443) and 1-(3-(dimethylamino)propyl)-3-ethylcarbodiimide hydrochloride (EDC) were purchased from Tokyo Chemical Industry Co., Ltd. (Tokyo, Japan). *N*-Hydroxysulfosuccinimide sodium salt (NHS; Catalog No. M01387), Ni-NTA agarose (Catalog No. 30230), and tris(2,2′-bipyridyl)dichlororuthenium(II) hexahydrate (Catalog No. 224758) were obtained from Meryer Chemical Technology Co., Ltd. (Shanghai, China), Qiagen (Hilden, Germany), and Sigma (St. Louis, MO), respectively. Restriction endonucleases and T4 DNA ligase were obtained from New England Biolabs (Ipswich, MA). Chemically competent cells of *E. coli* DH5α and BL21(DE3), TIANprep Mini Plasmid Kit and TIANgel Midi Purification Kit were purchased from TIANGEN Biotech (Beijing, China). Amicon Ultra-15 centrifugal filter units with Ultracel-3K and Ultracel-10K membranes, and dialysis tubing (3.5 kDa and 10 kDa molecular weight cutoff) were obtained from Millipore (Billerica, MA) and Spectrum Laboratories (Phoenix, AZ), respectively.

Construction of Expression Plasmids. Plasmids pET19b-R8 and pET19b-R32, previously developed for recombinant expression of 8 and 32 repeats of the resilin-like sequence (GGRPSDSYG-APGGGN) under the IPTG-inducible *T7* promoter,[22] were employed in this study. To express 64 repeats of the resilin-like sequence, plasmid pET19b-R64 was constructed by ligating the 2.4-kb, *Pvu*I-*Nhe*I fragment of plasmid pET19b-R32 with the 6.3-kb, *Spe*I-*Pvu*I fragment of pET19b-R32.

Protein Expression, Purification, and Identification. Each of the resilin expression plasmids was transformed into chemically competent cells of *E. coli* BL21(DE3), and plated onto a Luria−Bertani (LB) medium solidified with 1.5% agar and supplemented with 100 mg L^{-1} of ampicillin. The transformation plates were incubated overnight at 37 °C in a humidified incubator. The positive colonies harboring expression plasmids of interest were maintained as 15% (v/v) glycerol stocks at −80 °C.

Recombinant protein expression was performed in a 5 L jar fermentor (Biotech-5JG-7000; BaoXing Bio-Engineering Equipment, Shanghai, China) with fed-batch cultures. The seed culture was grown in shake flasks with a defined R/2 medium[34,35] containing 10 g L^{-1} of glucose and 100 mg L^{-1} of ampicillin at 37 °C. The flask cultures (200 mL) were then inoculated into the jar containing 2 L of the fresh R/2 medium at 37 °C until downshifted to 30 °C at the induction stage (see below). The culture pH was controlled at 6.80 by adding 30% ammonium hydroxide, except for the short periods of pH increase due to glucose depletion. The dissolved oxygen (DO) concentration was kept at 40% of air saturation by increasing the agitation speed from 200 to 800 rpm and by infiltrating pure oxygen. When DO rose to a value of greater than 70% due to glucose depletion, a feeding solution containing 700 g L^{-1} of glucose and 20 g L^{-1} of $MgSO_4{\cdot}7H_2O$ was added into the fermentor to increase the glucose concentration to ~1 g L^{-1}. When cell optical density at 600 nm (OD_{600}) reached ~50, the culture temperature was downshifted to 30 °C, and IPTG was added to a final concentration of 1 mM IPTG. The nutrient solution was then added to the jar using a pH-stat feeding strategy. After 6 h of cultivation, the induced cells were harvested by centrifugation and stored at −40 °C before use.

To purify recombinant proteins, the frozen cells were thawed on ice, resuspended in 20 mM Tris−HCl buffer (pH 8.0) containing 150 mM NaCl and 5 mM imidazole, and then lysed using a high-pressure homogenizer. The supernatant of the cell lysate was then used for affinity purification using a Ni-NTA agarose resin column. The eluted proteins with 250 mM imidazole were then dialyzed against water and concentrated using a centrifugal filter unit. Notably, a dialysis tubing with 3.5 kDa molecular weight cutoff, and Amicon Ultra-15 centrifugal filter with Ultracel-3K membrane were used for the processing of R8, which is relatively small in molecular weight (~16.4

DOI: 10.1021/acs.biomac.9b00389
Biomacromolecules 2019, 20, 3283−3293

kDa). For the processing of R32 and R64, the dialysis tubings with 10 kDa molecular weight cutoff, and Amicon Ultra-15 centrifugal filter units with Ultracel-10K membranes were used. The purity of the proteins was analyzed by 12% SDS-PAGE with Coomassie staining, and the protein solutions were quantified using the BCA Protein Assay Kit. The purified proteins were then freeze-dried.

The molecular weights of the purified proteins were confirmed by MALDI-TOF mass spectrometry. Briefly, 5 μL of each protein solution at 5 mg mL^{-1} was mixed with 25 μL of the matrix solution, which was prepared by dissolving sinapinic acid in 50:50 acetonitrile:-water with 0.1% trifluoroacetic acid to a concentration of 10 mg mL^{-1}. The protein samples (1 μL) were spotted on a polished steel target plate (massive target plate 384 type). Mass spectra were then collected on a Bruker Autoflex Speed MALDI-TOF mass spectrometer (Bruker Daltonics, Leipzig, Germany).

Preparation of Reduced Graphene Oxide (rGO)−Resilin Conjugate. The rGO-R64 conjugate was prepared by conjugating the terminal amino group of R64 to the carboxyl group of GO, followed by ascorbic acid reduction of the hydroxyl group of GO. First, 9.6 mg of EDC, 20 mg of GO, and 21.7 mg of NHS were sequentially dissolved in 10 mL of a 4-morpholineethanesulfonic acid buffer (100 mM, pH 6.0) with sonication. The mixture, which contained EDC, GO, and NHS at 5 mM, 2 mg mL^{-1}, and 10 mM, respectively, was stirred and allowed to react at room temperature for 30 min. After the mixture was adjusted to pH 7.5 by adding an equal volume of 200 mM phosphate buffer (pH 7.5), 200 mg of lyophilized R64 was added to initiate the conjugation reaction at room temperature for 2 h. Subsequently, the conjugation products were separated from excess EDC, EDC-byproducts, and NHS by using an Amicon Ultra-15 centrifugal unit with Ultracel-10K membrane, washed by deionized water for 5 times, and then reduced with 5 mM ascorbic acid at 85 °C for 1 h. The above reaction mixture was filtered through a 0.45 μm membrane, and the reduced GO-R64 conjugate was washed with deionized water and lyophilized. The product was then resuspended with 50 mM phosphate buffer (pH 7.2) containing 80% glycerol to a concentration of 8 mg mL^{-1}, and stored at −20 °C for future use.

Atomic Force Microscopy (AFM). AFM was performed in tapping mode using an Environment Control Scanning Probe Microscope system (Nanonavi E-Sweep, SII Nanotechnology Inc., Tokyo, Japan). Oxidized graphene, rGO-R64 conjugate, and a mixture of R64 and rGO were dissolved in deionized water, and ultrasonicated for 30 min at room temperature. 10 μL of each sample at 1 μg mL^{-1} was casted on mica surfaces and allowed to dry overnight at 37 °C. In all AFM experiments, a commercial silicon tip probe was used with a scanning rate of 1.7 Hz. The AFM images were collected with a scanning area of 2 μm × 2 μm and further processed with the NanoNavi II analysis software (SII Nano Technology Inc.).

Preparation of Hydrogels. Three types of hydrogels were prepared using the $[Ru(bpy)_3]^{2+}$-mediated photochemical cross-linking to form dityrosine cross-link networks. In one experiment, lyophilized proteins of R8, R32, or R64 were dissolved in 50 mM phosphate buffer (pH 7.2) with mild mixing and incubated for 30 min at 37 °C. Each protein solution was then mixed with ammonium persulfate and $[Ru(bpy)_3]^{2+}$ at final concentrations of 20 and 0.2 mM, respectively, and irradiated in a dumbbell mold for 3 min at 10 cm away from the samples with a 200 W white light source. In another experiment for the fabrication of adhesive protein hydrogels, glycerol was added at indicated concentrations before photochemical gelation in both dumbbell molds and rectangular molds. The hydrogels fabricated in the dumbbell molds were used for tensile tests, whereas the rectangular hydrogels were used for adhesive tests as described below. The third type of hydrogels, which were adhesive and electroconductive, were fabricated by incorporating rGO-R64 conjugate in the precursor protein solutions. Briefly, the lyophilized protein of pristine R64 was dissolved in the phosphate buffer, and mixed with the rGO-R64 stock solution and the photo-cross-linking agents as described above. The final concentrations of R64, rGO-R64, and glycerol in the mixture were approximately 200, 2 mg mL^{-1} (unless specified otherwise), and 20%, respectively.

Quantification of Dityrosine. The photochemical cross-linking degree of the hydrogels was evaluated by using a fluorescence-based method for quantification of dityrosine in hydrogel hydrolysates. Briefly, the hydrogels were immersed in deionized water with three times of water change to remove the photo-cross-linking agents and glycerol, and then freeze-dried. The lyophilized hydrogels (10 mg) were hydrolyzed in 2 mL of 6 M HCl supplemented with 10 μL of phenol at 110 °C for 22 h under nitrogen gas protection. The hydrolysates were blow-dried with nitrogen and then redissolved in 100 mM phosphate buffer (pH 7.2). An aliquot of the hydrolysate (200 μL) was transferred onto a 96-well quartz plate, and fluorescence (excitation 315 nm, emission 410 nm) was measured with an EnSpire 2300 plate reader (PerkinElmer, Waltham, MA). The dityrosine standard was dissolved and serially diluted in the same phosphate buffer for analysis. The cross-linking degree of dityrosine was presented as a percentage of determined level of dityrosine in the hydrogel hydrolysate to the stoichiometrical amount in the hydrogel.

Scanning Electron Microscopy (SEM). The first type of hydrogels that did not contain glycerol was briefly rinsed with 20 mM phosphate buffer (pH 7.2), whereas the other types of hydrogels were thoroughly washed with the above buffer at 37 °C to remove glycerol, which otherwise would adversely affect subsequent lyophilization. Subsequently, the hydrogels were frozen in liquid nitrogen for 10 min and lyophilized for 2 days using a Labconco FreeZone 4.5L lyophilizer (Labconco Corporation, Kansas City, MO). The specimens were then coated with gold using a Leica EM SCD050 sputtering device with a water-cooled sputter head (Leica Microsystems GmbH, Vienna, Austria). The SEM analyses were performed using a model S-3400N scanning electron microscope (Hitachi, Tokyo, Japan).

Mechanical Property Tests. All mechanical properties were measured on an Instron 5944 testing machine equipped with a 10 N load cell (Instron Corporation, Norwood, MA) at 25 °C and 60% relative humidity. Before tensile tests, the dumbbell-shaped hydrogels were coated with dimethylsilicone oil to minimize moisture evaporation, and wrapped with gauze and sandpaper at the two ends of the hydrogels to facilitate sample loading and gripping during testing. Cyclic loading−unloading tensile tests were performed at a speed of 2 mm min^{-1} and stretched to 100% strain with 3 continuously repeated cycles. The resilience of each sample was calculated from the first cycle test as the ratio of the area under the retraction curve to the extension curve. Moreover, tensile rupture tests were also performed for the hydrogels.

Adhesion Property Test. The adhesive strength of the hydrogels was investigated via the lap shear testing method with slight modifications. Fresh porcine skin was purchased from the local market, wiped with ethanol to remove fat contamination from skin epidermis, and cut into rectangular sections (20 mm in length and 60 mm in length). Then, a piece of 6 mm × 30 mm rectangular hydrogel was applied to the epidermis of the skin and sandwiched by the other piece of porcine skin with an overlapping area of 6 mm × 20 mm. The sample was pressed with a 100 g weight for 5 min at room temperature, and then lap-shear tested to failure at a speed of 2 mm min^{-1} on the Instron 5944 testing machine. The adhesive strength was calculated by dividing the maximum load by the area of the corresponding adhesive overlap. Three samples for each group were used in the adhesion tests.

Electrical Characterization. The electrical conductivity of the hydrogels was measured by a standard four-probe method with an ST2253 digital tester (Jingge Electronic Co., Ltd., Suzhou, China). The resistance of the hydrogel conductors was monitored using an HC 9205N digital multimeter (Huachuang Instrument Co., Ltd., Shenzhen, China). To test resistance variations while the hydrogels were stretched or compressed, the two ends of each rectangular hydrogel were wrapped with copper foils and connected with electrodes of the digital multimeter. The hydrogel conductors were then loaded onto the Instron 5944 machine and stretched with a constant rate of 2 mm min^{-1} at room temperature for recording the resistance change as a function of strain. Similarly, the resistance change upon pressure was recorded with the same setup, except that

DOI: 10.1021/acs.biomac.9b00389
Biomacromolecules 2019, 20, 3283−3293

the hydrogel was compressed on the universal testing machine. The electronic resistance variation ratio ($\Delta R/R_0$) was then quantified.

The amperometric current was monitored through a conventional three-electrode system using the CHI760E electrochemical workstation (Chenhua Instrumental Co., Shanghai China). The rectangular hydrogels were wrapped with copper foils at both ends for electrode connection, and then exposed to repeated cycles of stretching (100% strain) and relaxation. In another experiment, the hydrogels sensors were exposed to repeated cycles of compression (~9.8 kPa) and relaxation via imposing onto and lifting from the hydrogels a 50 g weight. The hydrogel sensors as described above were also adhered to a human index finger, and the amperometric current−time curves were monitored upon repeated cycles of bending and unbending of the finger. In addition, the sensors were attached to an Adam's apple, and the amperometric current−time curves were monitored while pronouncing the first author's surname "Hu" and given name "Xiao" repeatedly.

RESULTS AND DISCUSSION

Design and Biosynthesis of RLPs with Various Mw. We hypothesized that protein Mw is a critical structural feature that affects the mechanical properties of resulting RLP materials. To test this hypothesis, three genetically engineered RLPs were designed with varying numbers of resilin-like (GGRPSDSYGAPGGGN) blocks from the first exon of the fruitfly *D. melanogaster* CG15920 gene.[20,21] As described in our earlier study,[22] DNA sequence encoding four repeats of the resilin-like sequence was chemically synthesized and cloned into an expression plasmid (pET19b-R4). The construction of vectors that encode RLPs having more repetitive blocks was achieved by using the iterative polymerization strategy as described earlier.[34,35] Hence, expression plasmids were constructed that encode recombinant RLPs having 8−64 repeats of the resilin-like sequence (Figure 1a), with predicted molecular weights ranging from 16.37 to 93.51 kDa. Notably, the R64 protein had a theoretical molecular weight exceeding those of the full-length recombinant resilin of fruit fly (60 kDa),[23] and to the best of our knowledge represents the largest RLPs reported so far.

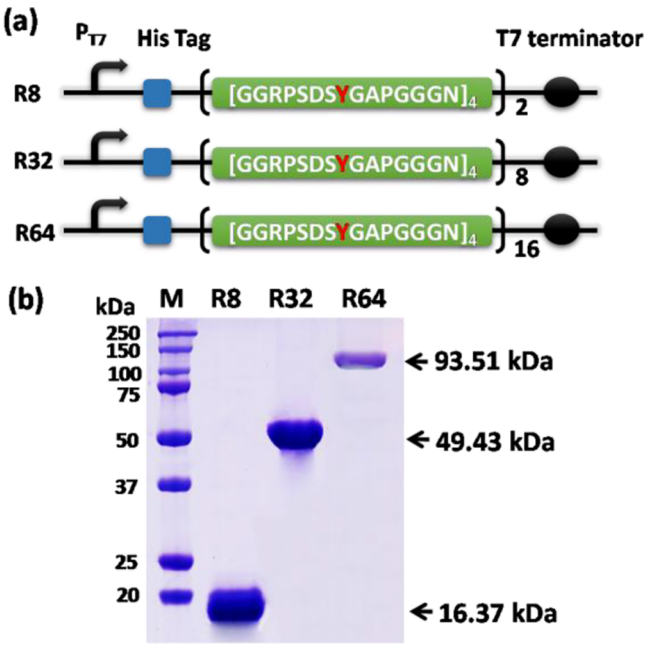

Figure 1. (a) Genetic constructs of recombinant R8, R32, and R64. (b) Coomassie-stained 12% SDS-PAGE gel analysis of the purified proteins. Arrows at the right indicate the respective theoretical molecular weights, which were calculated using the ProtParam tool (http://web.expasy.org/protparam/) and verified by mass spectrometry (see Figure S1).

The three RLPs were biosynthesized in recombinant *E. coli* and then purified as described in the Methods section. SDS-PAGE analysis revealed that all the purified protein polymers had purity greater than 95% (Figure 1b). These proteins were further verified by mass spectrometry, with determined molecular weights all within 0.72% difference of the expected theoretical values (Figure S1). The yields of the purified R8, R32, and R64 were approximately 530, 770, and 370 mg L^{-1} of bacterial culture, respectively. Here, the development of high cell density cultivation with minimal salts medium in bioreactor resulted in ~10-fold increase in the volumetric yield of R32 compared to that of flask cultivation with rich medium.[22] In addition, the biosynthetic strategy allowed production of the high molecular weight R64 at an appreciably high titer, which indicated general applicability of the strategy for preparing soluble recombinant resilin in large quantities.

Modulating Mechanical Properties of RLP Hydrogels by Varying Protein Mw. With the above three RLPs in hand, next we explored the relationship between protein Mw and the mechanical properties of RLP hydrogels. To this end, aqueous solutions of 26.5 wt % R8, 20 wt % R32, and 20 wt % R64, which contained tyrosine residues at comparable levels, were photochemically cross-linked. The resulting dumbbell-shaped hydrogels were tensile tested (Figure 2a). Interestingly, the strength of the hydrogels increased dramatically as the protein Mw increased, whereas the strain-at-break was inferior with an increase in the protein Mw. As a result, the ratio of stress to strain (stiffness) and toughness of the hydrogels increased greatly as the protein Mw was elevated. For example, the average stiffness of the R64 hydrogel (136.4 kPa) was ~18.2-fold higher than that of the R8 hydrogel, and the average toughness of the former hydrogel (107.6 kJ m^{-3}) was 4-fold higher than that of the latter hydrogel (Table 1). We also evaluated resilience of the three hydrogels by cyclic tensile tests. As shown in Figure 2b, negligible hysteresis was observed for these hydrogels upon stretching to 200% of their original length. Despite the huge difference in protein Mw before cross-linking, all these hydrogels had a resilience of at least 97.5% (Table 1), which was comparable to 97% resilience for Rec1-resilin[21] and 96% resilience for full-length recombinant resilin.[28]

As dityrosine cross-linking was critical in converting solution of soluble resilin into a supramolecular network, we evaluated the extent of dityrosine formation in the above three hydrogels. According to fluorescence-based quantification, these hydrogels had a similar degree of cross-linking, with about 46% of tyrosine residues occurring as the dityrosine dimer (Figure S2). To explore further the structure−property relationship, we performed scanning electron microcopy (SEM) analysis on these hydrogels and observed typical porous-like microstructures. However, the pore size and pore wall thickness of the R8 hydrogel appeared to be much smaller than those of the R32 and R64 hydrogels (Figure S3), indicating a link between protein Mw, hydrogel microstructures, and mechanical properties. Taken together, these results demonstrated that modulating the Mw of RLPs was an effective means to tune the mechanical properties of the dityrosine cross-linked hydrogels.

DOI: 10.1021/acs.biomac.9b00389
Biomacromolecules 2019, 20, 3283−3293

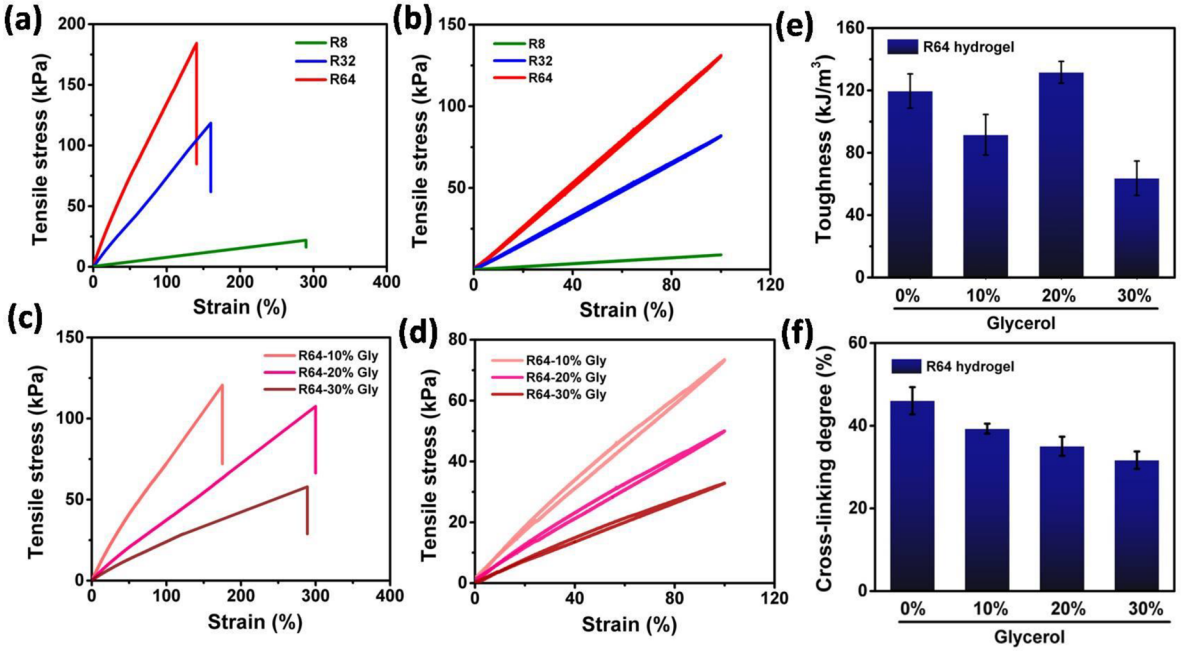

Figure 2. (a) Tensile stress−strain curves, and (b) cyclic tensile test curves of resilin hydrogels constructed from proteins with varying Mw. (c) Tensile stress−strain curves, and (d) cyclic tensile test curves of R64 hydrogels fabricated from protein solutions with varying levels of glycerol. Each cyclic tensile test was performed with three loading−unloading cycles and a strain at 100%. The toughness and cross-linking degree of the R64 hydrogels with and without glycerol addition are shown in panels e and f, respectively. Error bars indicate standard deviation of the data.

Table 1. Mechanical Properties of Resilin Hydrogels Fabricated in This Study

Hydrogel	Strain at break (%)	Strength (kPa)	Stiffness (kPa)	Toughness (kJ m^{-3})	Resilience[a] (%)
R8	264.4 ± 25.5	20.0 ± 1.9	7.5 ± 1.7	26.7 ± 5.0	98.5 ± 1.5
R32	144.7 ± 10.4	123.7 ± 4.3	85.2 ± 5.3	88.6 ± 2.2	99.7 ± 0.5
R64	127.9 ± 12.9	169.8 ± 14.6	136.4 ± 4.7	107.6 ± 22.2	97.5 ± 0.5
R64-20% glycerol	294.3 ± 16.2	96.4 ± 7.2	36.7 ± 2.2	180.5 ± 19.5	98.1 ± 1.4
Hybrid hydrogel[b]	326.5 ± 27.4	88.7 ± 3.0	44.3 ± 2.3	212.7 ± 27.3	82.4 ± 2.2

[a]Resilience was calculated from the ratio of the area under the relaxation curve to the area under the stretching curve at a strain of 100%. [b]The hybrid hydrogel was fabricated with rGO-R64, pristine R64, and glycerol at 2, 200 mg mL^{-1}, and 20% (w/v), respectively.

The mechanical properties of elastomeric networks from tandem-repeat proteins can be simulated using elasticity theory models.[21,36−38] The stress−strain data have been previously used to estimate the cross-link density using the statistical theory of rubber-like elasticity.[21] In a similar manner, the molecular mass between cross-links (M_c) was estimated for our R8, R32, and R64 hydrogels (Figure S4). The results indicated that M_c increased with the number of resilin-like repeats, and the increased density of cross-linked chains resulted in resilin networks with higher moduli and toughness.

Modulating Mechanical and Adhesive Properties by Adjusting Solvents. To expand further the mechanical versatility of the RLP materials, we investigated the effects of adjusting solvents in the protein solutions before photochemical cross-linking. It is well-known that glycerol is more viscous than water, and forms strong hydrogen bonds with water molecules.[15] Therefore, we hypothesized that the addition of glycerol and other multihydroxyl compounds in the pregelation solutions might plasticize the resulting hydrogels. To test the hypothesis, glycerol, ethylene glycol, and polyethylene glycol 200 (PEG 200) were individually added to the pregelation solution of R64, which was shown as a typical example, and the resulting hydrogels were tensile tested. Indeed, the addition of all these multihydroxyl compounds significantly improved hydrogel extensibility, with a 1.5- to 2.7-fold increase in the strain-at-break (Figure S5a) when compared with the control R64 hydrogel at ∼127.9% (Table 1). The exciting result prompted us to study the effects of multihydroxyl compounds in more details.

Next, we tested the effect of addition level on the mechanical properties of hydrogels. As a typical multihydroxyl compound, glycerol was chosen and added at a final concentration of 10−30% to the pregelation solution of R64 for hydrogel fabrication. Based on tensile testing, the strength of the R64 hydrogels was consistently decreased with an increase in the addition level of glycerol. The extensibility of these glycerol-containing hydrogels was improved when compared with the control R64 hydrogel without glycerol (Figure 2c). Notably, addition of 20% glycerol resulted in the best extensibility, with a strain-at-break of ∼300%. In addition, only small hysteresis was observed for these hydrogels upon stretching to 200% of their original length (Figure 2d), with resilience estimated to be over 95%. In general, the hydrogel toughness appeared to be inferior with an increase in glycerol concentration (Figure 2e), which was attributed at least partially to the compromised effect of glycerol addition on photochemical cross-linking (Figure 2f). However, the toughness of the R64 hydrogel with 20% glycerol was significantly higher than that of the control

DOI: 10.1021/acs.biomac.9b00389
Biomacromolecules 2019, 20, 3283−3293

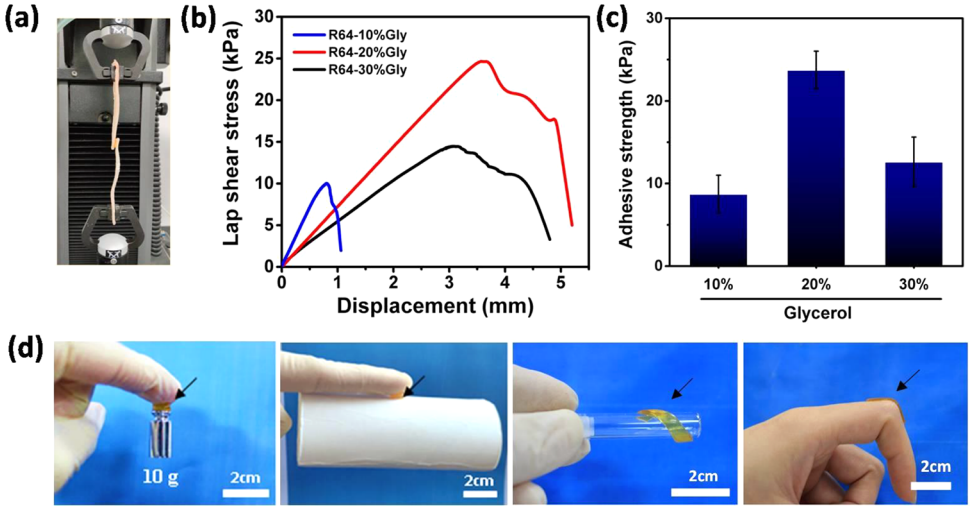

Figure 3. Adhesive behavior of R64-glycerol hydrogels. (a) Experimental setup, (b) lap shear stress vs displacement curves, and (c) adhesion strength of the hydrogels on porcine skin. For clarity, the control hydrogel without glycerol was not shown as its adhesive strength was undetectable. (d) Photographs of the R64-20% glycerol hydrogel adhering to various substrates. Note that photochemical cross-linking was necessary for gelation from the R64 solutions supplemented with 10−30 wt % glycerol.

R64 hydrogel (Table 1). This result was surprising and might be explained by the fact that even though the hydrogel strength was decreased the hydrogel extensibility was disproportionally improved under the optimal level (20%) of glycerol addition. Taken together, the above results demonstrated that incorporation of multihydroxyl compound in the pregelation solution was effective to modulate the mechanical properties of the resulting hydrogels.

Interestingly, the R64-glycerol hydrogels adhered to the authors' finger in handling, which prompted us to study whether the incorporation of glycerol endowed adhesive properties to the hydrogels. To this end, lap shear testing was performed using the standard ASTM F2255-05 method[39] with fresh porcine skin surfaces as substrates (Figure 3a). The stress-displacement curves were recorded for the hydrogels with varying levels of glycerol (Figure 3b). The maximal detachment stress, termed adhesive strength, was then derived from each stress-displacement curve. It should be noted that the adhesive strength of the control R64 hydrogel was negligible (data not shown), and the hydrogels with glycerol exhibited adhesive strength in an addition dose-dependent manner (Figure 3c). Within the wide range of levels tested, addition of 20% glycerol resulted in the largest increase in hydrogel adhesive strength, reaching an appreciably high level of 23.8 ± 2.3 kPa. In addition to skin tissues, the R64-20% glycerol hydrogels can also adhere to substrate surfaces such as metals, rubber gloves, glass, and cellulosic products (Figure 3d). Furthermore, we found that the addition of ethylene glycol and PEG 200 also endowed adhesive properties, albeit to a less extent compared to the addition of glycerol (Figure S5b). These results indicated that incorporation of multihydroxyl compounds might be a generally effective approach to endow adhesiveness to the RLP hydrogels.

To explore the molecular mechanisms, we characterized R64 in solutions without and with glycerol at various levels. In all the solutions, the protein showed a disordered structure (Figure S6a). The R64 solution without glycerol revealed nanostructures with a hydrodynamic diameter of ∼150 nm, indicating the formation of supramolecular assemblies. Such assemblies with larger diameters were observed as the glycerol level increased (Figure S6b). Concomitantly, the intensity of tyrosine fluorescence was decreased from these protein nanostructures with larger diameters (Figure S6c). Clearly, the exposure of the tyrosine residues available for cross-linking was masked due to the enhancing effect of glycerol on R64 assembly, which coincided well with the reduced efficiency of cross-linking (Figure 2F).

We surmised that glycerol might have two roles in adhesion. On one hand, with the large number of hydroxyl groups, glycerol may be directly involved in the formation of hydrogen bonds with the skin tissue to endow adhesion.[15] On the other hand, as assembly of R64 was enhanced by glycerol in precursor solutions, the resulting cross-linked hydrogels might have differing amino acid motifs exposed to interfaces, and these motifs contributed to adhesion to the tissue substrate via hydrophobic, cation−π, and other possible interactions. The two possible roles may explain why adhesion was seen at all levels of glycerol addition, yet with the optimal at 20%. Nonetheless, the detailed mechanisms for adhesion are still unclear and deserve further investigations.

Endowing Electroconductive Properties with Graphene−Resilin Conjugate. To endow electroconductive properties, we initially added graphene to the pregelation solution of R64 for hydrogel fabrication. However, the resulting hydrogels were undesirable as they are mechanically and electronically unstable under large tensile strains (Figure S7). It was possible that the sheets of graphene slid along the graphene/resilin network interfaces under large deformation because the graphene sheets were not firmly anchored to the hydrogel network. To tackle this problem, we attempted to conjugate resilin to the sheets of graphene, and cross-link the resulting graphene−resilin conjugate with pristine resilin to form a hybrid hydrogel network.

The rGO-R64 conjugate was synthesized via the carbodiimide coupling reaction[40] using EDC·HCl and NHS as described in the Methods section. To observe its microscopic structures, atomic force microscopy (AFM) analysis was performed (Figure 4). As a control, the starting substrate GO exhibited typical layer structures with smooth, flat surfaces. However, rough surfaces were observed from the graphene

DOI: 10.1021/acs.biomac.9b00389
Biomacromolecules 2019, 20, 3283−3293

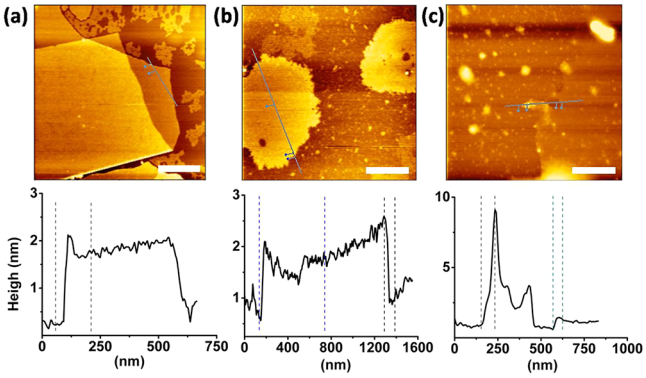

Figure 4. Representative AFM images of the microstructures for (a) oxidized graphene, (b) rGO-R64 conjugate, and (c) a mixture of unconjugated R64 and rGO. Freshly prepared suspension (10 μL) in deionized water at a concentration of 10 μg mL^{-1} was casted on mica surfaces and allowed to dry at 37 °C before AFM analysis. Scale bar: 500 nm.

sheets of the rGO-R64 conjugate. In addition, the edges of the graphene sheets of rGO-R64 were ∼0.6 nm thicker than the middle positions of the sheets, which might be due to that the R64 protein was anchored to the edges of the sheets as the carboxyl groups usually existed at the edges of GO sheets. For the simple mixture of rGO and R64, we observed large quantities of aggregates of the protein with sizes varying from 10 to 100 nm. In addition, the aggregates of the protein were found to distribute randomly on the sheets of rGO, indicating that the protein might be adsorbed on the graphene sheets through nonspecific interactions.

To analyze surface chemistry, X-ray photoelectron spectroscopy (XPS) analyses were performed for rGO, the rGO-R64 conjugate, and rGO with nonspecifically adsorbed R64 (Figure S8). As expected, the appearance of a nitrogen peak (N 1s) was observed in the conjugate but not in rGO. In addition, low levels of oxygen functional groups in rGO indicated incomplete removal of these groups during ascorbic acid reduction of GO, which was also reported earlier.[41] These groups may be involved in nonspecific interaction with R64, leading to a certain level of R64 absorption onto rGO. Although XPS did not reveal any difference in chemical bonds between samples of chemical conjugation and nonspecific adsorption, the analyses indicated that more proteins were chemically conjugated compared with nonspecific adsorption.

The characterized rGO-R64 conjugate was then added at various levels for fabrication of hybrid hydrogels by photochemical cross-linking (Figure 5a). As expected, hybrid hydrogels were obtained with the addition of rGO-R64 at levels up to 2 mg mL^{-1}. However, a self-supporting hydrogel did not form with 4 mg mL^{-1} and higher levels of the conjugate. This was possibly due to insufficient cross-linking because a high level of rGO-R64 may shield light penetration into the precursor solution for photo-cross-linking. The hydrogel with 2 mg mL^{-1} of rGO-R64 is hereafter termed as "the hybrid hydrogel" and shown as a typical example for detailed characterization. The hybrid hydrogel could be stretched up to 4.5 times of its original length without failure, and possessed a stress-at-break value of ∼90 kPa (Figure 5b). Under low strain condition (20% strain), the hybrid hydrogel was highly recoverable (Figure 5c), with resilience estimated to be 90%. However, the hydrogel was less recoverable under large strains (60% strain and higher), and was shown to be 82.4 ± 2.2% resilient when stretched to two times of its original length (Table 1). This resilience performance was comparable to that of high-resilience polybutadiene rubber (80%), and far superior to that of the low-resilience chlorobutyl rubber (56%).[21] As proposed earlier, the physical properties of rec1-resilin were attributed to the three-dimensional (3D) amorphous nature of the dityrosine cross-linked protein matrix and the role of water as plasticizer, as dehydrated resilin became very glassy and brittle, and it was leathery with poor resilience in a partially dry environment (70% relative humidity).[21] When our hybrid hydrogel was incubated at 50% relative humidity and 37 °C for 3 days, it was

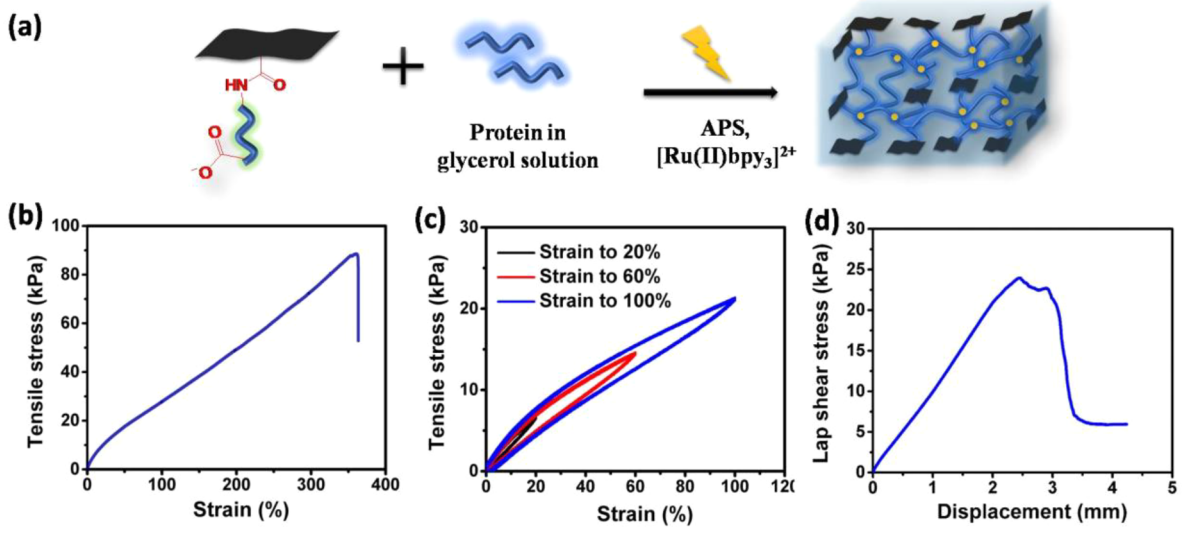

Figure 5. Mechanical and adhesive properties of rGO-R64-glycerol hydrogel. (a) Fabrication scheme, (b) tensile stress−strain curve, (c) cyclic tensile test curves, and (d) lap shear stress vs displacement curve of the hydrogel on porcine skin. A suspension of rGO-R64 conjugate, pristine R64, and glycerol at 2, 200 mg mL^{-1}, and 20% (w/v) was mixed with the photochemical cross-linking reagents and irradiated with white light to form the hydrogel.

DOI: 10.1021/acs.biomac.9b00389
Biomacromolecules 2019, 20, 3283−3293

only partially dehydrated (about 32%) while maintaining the tensile and resilient properties (Figure S9).

In addition to be mechanically stretchable and resilient, the hybrid hydrogel was also adhesive as it self-adhered to various surfaces such as human finger skin, latex, and glass (Figure S10 and Video S1, Supporting Information). Based on the lap shear test, the hybrid hydrogel was shown to have a high adhesion strength of ~24 kPa (Figure 5d), which was comparable to that of the R64-20% glycerol hydrogel. This result indicated that the incorporation of the rGO-R64 conjugate did not compromise hydrogel adhesiveness as long as glycerol was added at comparable levels.

The above hybrid hydrogel and the R64-20% glycerol hydrogel, which served as a control for comparison, were processed for SEM analysis. As these hydrogels cannot be completely freeze-dried due to the incorporation of glycerol, the hydrogel samples were first washed in a phosphate buffer to remove glycerol and then lyophilized for SEM analysis. As shown in Figure 6a, the R64-20% glycerol hydrogel showed

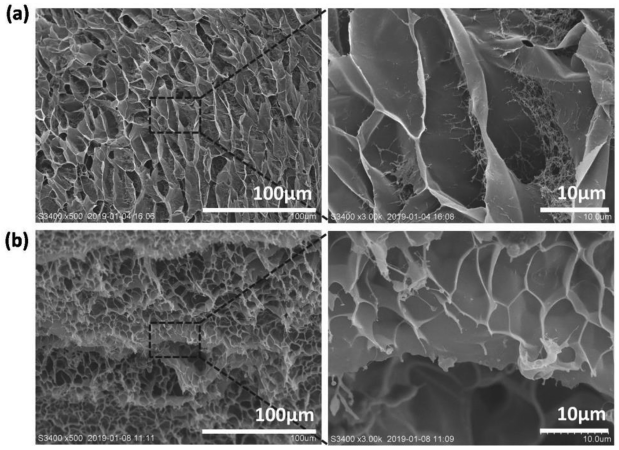

Figure 6. Scanning electron microscopy (SEM) of (a) R64-20% glycerol hydrogel, and (b) the hybrid hydrogel fabricated with rGO-R64, pristine R64, and 20% glycerol.

interconnected, porous-like structures. A closer inspection of the SEM image revealed microfibrils that were entangled within the pores of the hydrogel, which might be due to the un-cross-linked chains of the R64 protein since the glycerol addition decreased the degree of dityrosine cross-linking (Figure 2f). In contrast, we observed morphologies with layers of porous structures in the hybrid hydrogel (Figure 6b). The continuous, dense layers were formed as a result of rGO-R64 addition, possibly via stacking of the graphene sheets. These ordered microstructures coincided well with the robust mechanical properties of the hydrogel.

Next, we evaluated the electroconductive properties of the hybrid hydrogel. According to a standard four-probe method with a digital tester, the electrical conductivity of the hybrid hydrogel was determined to be 0.92 ± 0.08 S m^{-1} (Figure S11), which was well above the benchmark of 0.1 S m^{-1} desired for use in electrochemical devices.[42] Due to its good extensibility and conductivity, the electronic properties of the hybrid hydrogel were assessed under mechanical deformations. In one investigation, the electrical resistance of a specimen of the hydrogel under an applied strain was recorded by loading the specimen on a universal tensile machine. The relationship between the relative resistance change ($\Delta R/R_0$) and the applied strain (ε) is shown in Figure 7a. Remarkably, a linear relation between $\Delta R/R_0$ and ε was observed in the wide range

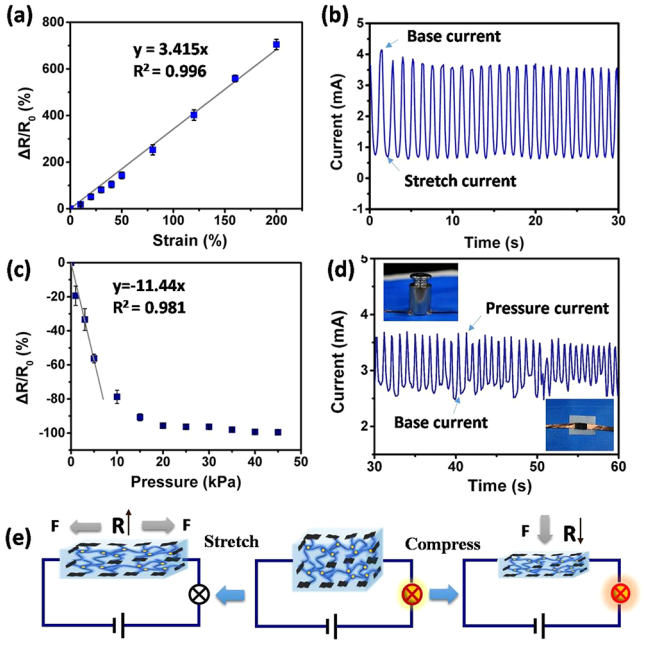

Figure 7. Strain- and piezo-dependent electrical conductivity of the hybrid hydrogel. (a) The relative resistance change upon tensile strain. (b) Time profile of current under stretching−relaxation cycles with a tensile strain at 100%. (c) The relative resistance change upon pressure. (d) Time profile of current under loading−unloading cycles with a pressure at 9.8 kPa, which was generated by imposing a 50 g weight on the 1.0 × 0.5 cm^2 hydrogel. The insets are images of the hydrogel with and without weight imposing. (e) Scheme illustrates an increase in resistance of the hydrogel upon stretching, and a decrease in resistance upon pressing. In panels a and c, fitted straight lines based on linear regression are shown.

of strains up to 200%. The important stain parameter, gauge factor (GF), which is defined as $(\Delta R/R_0)/\varepsilon$, was determined to be 3.415, which was far superior to that of the graphene/silk fibroin nanocomposite film (with GF up to 0.47).[12] In addition, the electrical current through the hydrogel specimen, which was reciprocal of its electrical resistance, decreased synchronously upon a tensile strain to 100%, and recovered the original level upon relaxation in a cyclic manner (Figure 7b). The highly reliable monitoring of 100% strain, which is relevant to largescale human activities such as stretching, torsion, and bending of human limbs,[43] was desirable because this feature remains a major challenge in protein-based conductive materials, especially for use as strain sensors.

In another investigation, the electrical resistance of the hybrid hydrogel was found to decrease dramatically with an elevation in the applied pressure until a plateau level was reached (Figure 7c). The pressure sensitivity of the hydrogel resistance was ~0.11 kPa^{-1} under a relatively small pressure range from 0 to 10 kPa, which approximated gentle touch of human skin.[44] Similarly, smooth and recoverable changes in the electrical current were observed for the hydrogel under loading−unloading cycles with a pressure at 9.8 kPa (Figure 7d). The results implied that the hydrogel material might be used as piezoresistive stress sensors for subtle pressure sensing on human skin.

DOI: 10.1021/acs.biomac.9b00389
Biomacromolecules 2019, 20, 3283−3293

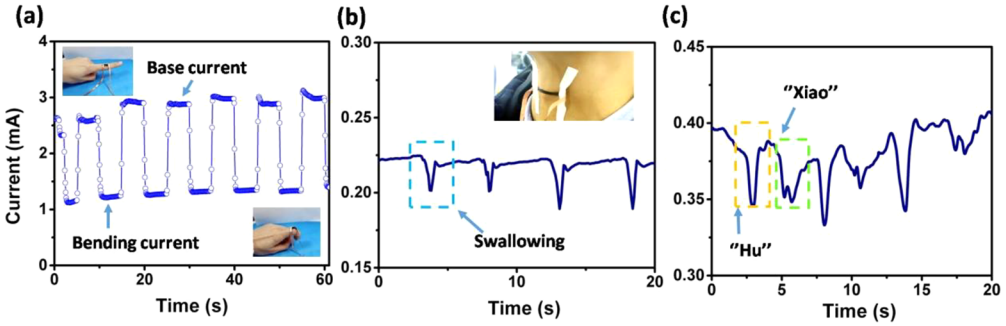

Figure 8. Real-time monitoring of human activities using the hybrid hydrogel sensor. (a) Signal detected for the repeated, fast bending and straightening of a human index finger. Insets are images of the sensor at straightening and bending states, respectively. When the sensor was attached to an Adam's apple, signals were detected for repeated (b) swallowing and (c) pronouncing "Hu" and "Xiao".

Obviously, the electroconductive properties of the hybrid hydrogel were attributed to the rGO-R64 conjugate that was cross-linked with the pristine R64. The stretching-triggered decrease and compression-induced increase in electroconductivity was intriguing, as shown by stretching and pressing the hydrogel network to turn "OFF" and "ON" lights in closed circuits (Figure S12 and Video S2). It was reasoned that the neighboring sheets of rGO constituted conductive fillers to enable transfer of electrical charges. The average distance between neighboring sheets of rGO were increased upon stretching of the hybrid hydrogel, which resulted in an increase in the electronic resistance and thus a decrease in the electroconductivity (Figure 7e). In contrast, the average distance between neighboring sheets of rGO was shortened upon compression, thus leading to an increase in the electroconductivity until the distance cannot be shortened any more due to the inherent limitation in hydrogel compression.

Furthermore, we explored whether the adhesive and electroconductive hydrogel could be used as wearable strain sensors for monitoring human activities. As a proof-of-concept, the hydrogel was initially employed to monitor macro-scale movements such as finger bending. As shown in Figure 8a, the hydrogel can be readily self-adhered to the rough skin of the finger knuckle, and repeated bending and extending of the finger did not disconnect the hydrogel. In addition, the periodic changes of current signal upon bending and extending stimuli could be monitored in real time. The hydrogel sensor was also applied for the monitoring of small-scale activities such as swallowing and phonating. To this end, the hydrogel was adhered to a volunteer's Adam's apple, and the connecting electric wires were attached on the volunteer's throat with tapes. As illustrated in Figure 8b, a very clear signal of current was generated, and the amplitude of the current varied moderately, which coincided with the uncontrollable variance in the movement amplitude of swallowing by the volunteer. Furthermore, the hydrogel sensor enabled high-resolution detection of the vibrations from vocal cords when the volunteer said "Hu" and "Xiao" repeatedly (Figure 8c). More interestingly, the monosyllabic and two-syllable words were accurately converted into distinct electrical signals with characteristic configurations. The encouraging results indicate the fast response and high sensitivity of the hydrogel sensors in monitoring subtle human activities. These features will meet the application needs of a variety of human-skin related fields such as healthcare bioelectronics and human–computer user interfaces.

The stability of the developed sensors is an important factor that may restrict their broad uses. This is particularly true for protein hydrogel-based sensors, since they are composed of 3D cross-linked networks of hydrophilic protein polymers with the capacity to retain a large amount of water. With glycerol incorporation, our hydrogel sensor escaped "drying out" at the human body temperature and a partially dry environment, the conditions of which are relevant to human skin. Although partially dehydrated under the above conditions, the sensor was mechanically stable (Figure S9). In addition, it was electromechanically sensitive enough to monitor stretching–relaxation cycles, although the sensitivity was moderately decreased (Figure S13). These initial efforts indicate that protein-based hydrogels could and should be further manipulated with improved stabilities for durable use in bioelectronics.

CONCLUSIONS

In summary, we have demonstrated the development of a hybrid graphene/resilin hydrogel that is simultaneously adhesive, electroconductive, and mechanically robust. The multiple desirable features were integrated into one hydrogel network by rational design of the graphene–resilin conjugate for cross-linking with pristine resilin from precursor solutions with the glycerol-water binary solvent. Such material design allows full exploitation of the instinctive features of the rubber-like biomaterial, resilin, which is famous for exceptional resilience (recovery after deformation), high strain, and low stiffness. Of particular interest, varying the Mw of genetically engineered RLPs enabled the fabrication of resilient hydrogels with protein Mw-dependent strength and stiffness, thus offering a strategy to modulate mechanical properties. Besides, adjusting solvent with the addition of glycerol to the precursor protein solutions was found to be another useful strategy to modulate mechanical properties. Notably, the glycerol–water binary solvent endowed hydrogels with adhesive properties that were strong enough to support self-attachment to diverse surfaces. Furthermore, the hybrid hydrogel exhibited recoverable electroconductivity that is sensitively and fast responsive to compression or strain deformations, thus enabling real-time monitoring of human activities as wearable sensors. The newly developed resilin-based conductive hydrogels are anticipated to find broader application in flexible electronics.

DOI: 10.1021/acs.biomac.9b00389
Biomacromolecules 2019, 20, 3283–3293

■ ASSOCIATED CONTENT

Supporting Information

The Supporting Information is available free of charge on the ACS Publications website at DOI: 10.1021/acs.biomac.9b00389.

Mass spectroscopy analysis of the purified protein polymers (Figure S1), the degree of dityrosine cross-linking and SEM images for the hydrogels with varying protein Mw (Figures S2 and S3), model fitting analysis (Figure S4), mechanical and adhesive properties of the R64 hydrogels with solvent adjustment (Figure S5), characterization of R64 solutions with glycerol (Figure S6), tensile and electrical properties of R64/graphene hydrogels (Figure S7), XPS analysis of the rGO-R64 conjugate (Figure S8), mechanical stability (Figure S9), illustrations of the adhesive behavior (Figure S10), electroconductivity of hydrogels with various levels of rGO-R64 (Figure S11), illustrations of strain- and piezo-sensitive electroconductivity (Figure S12), and electro-mechanical stability of the sensor (Figure S13) (PDF)

Illustration of the hybrid hydrogel adhered to two fingers in extension (Video S1) (MP4)

Fast responsive and recoverable electroconductivity for the hybrid hydrogel (Video S2) (MP4)

■ AUTHOR INFORMATION

Corresponding Author

*Z.-G. Qian. E-mail: zgqian@sjtu.edu.cn.

ORCID

Xiao-Xia Xia: 0000-0001-8375-1616

Zhi-Gang Qian: 0000-0002-0133-0605

Author Contributions

†X.H. and X.-X.X. contributed equally to this work.

Notes

The authors declare no competing financial interest.

■ ACKNOWLEDGMENTS

Financial support was provided by the National Natural Science Foundation of China (21674061 and 21406138) and The National Key Research and Development Program of China (2016YFE0204400). X.-X.X. acknowledges the program for professor special appointment at Shanghai institutions of higher learning. The authors acknowledge Xue-Lin Xia and Fang Pan for assistance as volunteers in the conductivity and adhesive tests.

■ REFERENCES

(1) Torculas, M.; Medina, J.; Xue, W.; Hu, X. Protein-Based Bioelectronics. *ACS Biomater. Sci. Eng.* **2016**, *2*, 1211−1223.

(2) Zhou, Z.; Zhang, S.; Cao, Y.; Marelli, B.; Xia, X.; Tao, T. H. Engineeringthe Future of Silk Materials through Advanced Manufacturing. *Adv. Mater.* **2018**, *30*, 1706983.

(3) Zhang, Y. Z.; Lee, K. H.; Anjum, D. H.; Sougrat, R.; Jiang, Q.; Kim, H.; Alshareef, H. N. MXenes Stretch Hydrogel Sensor Performance to New Limits. *Sci. Adv.* **2018**, *4*, No. eaat0098.

(4) Yuk, H.; Lu, B.; Zhao, X. HydrogelBioelectronics. *Chem. Soc. Rev.* **2019**, *48*, 1642−1667.

(5) Zhu, B.; Wang, H.; Leow, W. R.; Cai, Y.; Loh, X. J.; Han, M. Y.; Chen, X. SilkFibroin for Flexible Electronic Devices. *Adv. Mater.* **2016**, *28*, 4250−4265.

(6) Jo, M.; Min, K.; Roy, B.; Kim, S.; Lee, S.; Park, J. Y.; Kim, S. Protein-Based Electronic Skin Akin to Biological Tissues. *ACS Nano* **2018**, *12*, 5637−5645.

(7) Wang, L.; Chen, D.; Jiang, K.; Shen, G. NewInsights and Perspectives into Biological Materials for Flexible Electronics. *Chem. Soc. Rev.* **2017**, *46*, 6764−6815.

(8) Wang, C.; Li, X.; Gao, E.; Jian, M.; Xia, K.; Wang, Q.; Xu, Z.; Ren, T.; Zhang, Y. CarbonizedSilk Fabric for Ultrastretchable, Highly Sensitive, and Wearable Strain Sensors. *Adv. Mater.* **2016**, *28*, 6640−6648.

(9) Steven, E.; Saleh, W. R.; Lebedev, V.; Acquah, S. F. A.; Laukhin, V.; Alamo, R. G.; Brooks, J. S. CarbonNanotubes on a Spider Silk Scaffold. *Nat. Commun.* **2013**, *4*, 2435.

(10) Wang, E.; Desai, M. S.; Lee, S. W. Light-Controlled Graphene-Elastin Composite Hydrogel Actuators. *Nano Lett.* **2013**, *13*, 2826−2830.

(11) Annabi, N.; Shin, S. R.; Tamayol, A.; Miscuglio, M.; Bakooshli, M. A.; Assmann, A.; Mostafalu, P.; Sun, J. Y.; Mithieux, S.; Cheung, L.; Tang, X. S.; Weiss, A. S.; Khademhosseini, A. HighlyElastic and Conductive Human-Based Protein Hybrid Hydrogels. *Adv. Mater.* **2016**, *28*, 40−49.

(12) Ling, S.; Wang, Q.; Zhang, D.; Zhang, Y.; Mu, X.; Kaplan, D. L.; Buehler, M. J. Integrationof Stiff Graphene and Tough Silk for the Design and Fabrication of Versatile Electronic Materials. *Adv. Funct. Mater.* **2018**, *28*, 1705291.

(13) Kadumudi, F. B.; Jahanshahi, M.; Mehrali, M.; Zsurzsan, T. G.; Taebnia, N.; Hasany, M.; Mohanty, S.; Knott, A.; Godau, B.; Akbari, M.; Dolatshahi-Pirouz, A. AProtein-Based, Water-Insoluble, and Bendable Polymer with Ionic Conductivity: A Roadmap for Flexible and Green Electronics. *Adv. Sci.* **2019**, *6*, 1801241.

(14) Yao, M.; Su, D.; Wang, W.; Chen, X.; Shao, Z. Fabricationof Air-Stable and Conductive Silk Fibroin Gels. *ACS Appl. Mater. Interfaces* **2018**, *10*, 38466−38475.

(15) Han, L.; Liu, K.; Wang, M.; Wang, K.; Fang, L.; Chen, H.; Zhou, J.; Lu, X. Mussel-Inspired Adhesive and Conductive Hydrogel with Long-Lasting Moisture and Extreme Temperature Tolerance. *Adv. Funct. Mater.* **2018**, *28*, 1704195.

(16) Jing, X.; Mi, H. Y.; Lin, Y. J.; Enriquez, E.; Peng, X. F.; Turng, L. S. HighlyStretchable and Biocompatible Strain Sensors Based on Mussel-Inspired Super-Adhesive Self-Healing Hydrogels for Human Motion Monitoring. *ACS Appl. Mater. Interfaces* **2018**, *10*, 20897−20909.

(17) Shao, C.; Wang, M.; Meng, L.; Chang, H.; Wang, B.; Xu, F.; Yang, J.; Wan, P. Mussel-Inspired Cellulose Nanocomposite Tough Hydrogels with Synergistic Self-Healing, Adhesive, and Strain-Sensitive Properties. *Chem. Mater.* **2018**, *30*, 3110−3121.

(18) Wang, Z.; Chen, J.; Cong, Y.; Zhang, H.; Xu, T.; Nie, L.; Fu, J. UltrastretchableStrain Sensors and Arrays with High Sensitivity and Linearity Based on Super Tough Conductive Hydrogels. *Chem. Mater.* **2018**, *30*, 8062−8069.

(19) Zhou, Y.; Wan, C.; Yang, Y.; Yang, H.; Wang, S.; Dai, Z.; Ji, K.; Jiang, H.; Chen, X.; Long, Y. HighlyStretchable, Elastic, and Ionic Conductive Hydrogel for Artificial Soft Electronics. *Adv. Funct. Mater.* **2019**, *29*, 1806220.

(20) Ardell, D. H.; Andersen, S. O. TentativeIdentification of a Resilin Gene in *Drosophila melanogaster*. *Insect Biochem. Mol. Biol.* **2001**, *31*, 965−970.

(21) Elvin, C. M.; Carr, A. G.; Huson, M. G.; Maxwell, J. M.; Pearson, R. D.; Vuocolo, T.; Liyou, N. E.; Wong, D. C.; Merritt, D. J.; Dixon, N. E. Synthesisand Properties of Crosslinked Recombinant Pro-resilin. *Nature* **2005**, *437*, 999−1002.

(22) Huang, S. C.; Qian, Z. G.; Dan, A. H.; Hu, X.; Zhou, M.-L.; Xia, X. X. Rational Design and Hierarchical Assembly of a Genetically Engineered Resilin-Silk Copolymer Results in Stiff Hydrogels. *ACS Biomater. Sci. Eng.* **2017**, *3*, 1576−1585.

(23) Qin, G.; Lapidot, S.; Numata, K.; Hu, X.; Meirovitch, S.; Dekel, M.; Podoler, I.; Shoseyov, O.; Kaplan, D. L. Expression, Cross-linking, and Characterization of Recombinant Chitin Binding Resilin. *Biomacromolecules* **2009**, *10*, 3227−3234.

(24) Lyons, R. E.; Nairn, K. M.; Huson, M. G.; Kim, M.; Dumsday, G.; Elvin, C. M. Comparisonsof Recombinant Resilin-like Proteins: Repetitive Domains are Sufficient to Confer Resilin-like Properties. *Biomacromolecules* **2009**, *10*, 3009−3014.
(25) Lyons, R. E.; Wong, D. C.; Kim, M.; Lekieffre, N.; Huson, M. G.; Vuocolo, T.; Merritt, D. J.; Nairn, K. M.; Dudek, D. M.; Colgrave, M. L.; Elvin, C. M. Molecularand Functional Characterisation of Resilin Across Three Insect Orders. *Insect Biochem. Mol. Biol.* **2011**, *41*, 881−890.
(26) Li, L.; Teller, S.; Clifton, R. J.; Jia, X.; Kiick, K. L. TunableMechanical Stability and Deformation Response of a Resilin-Based Elastomer. *Biomacromolecules* **2011**, *12*, 2302−2310.
(27) Li, L.; Tong, Z.; Jia, X.; Kiick, K. L. Resilin-like Polypeptide Hydrogels Engineered for Versatile Biological Function. *Soft Matter* **2013**, *9*, 665−673.
(28) McGann, C. L.; Levenson, E. A.; Kiick, K. L. Resilin-Based Hybrid Hydrogels for Cardiovascular Tissue Engineering. *Macromol. Chem. Phys.* **2013**, *214*, 203−213.
(29) Qin, G.; Rivkin, A.; Lapidot, S.; Hu, X.; Preis, I.; Arinus, S. B.; Dgany, O.; Shoseyov, O.; Kaplan, D. L. RecombinantExon-Encoded Resilins for Elastomeric Biomaterials. *Biomaterials* **2011**, *32*, 9231−9243.
(30) Qin, G.; Hu, X.; Cebe, P.; Kaplan, D. L. Mechanismof Resilin Elasticity. *Nat. Commun.* **2012**, *3*, 1003.
(31) Dutta, N. K.; Truong, M. Y.; Mayavan, S.; Choudhury, N. R.; Elvin, C. M.; Kim, M.; Knott, R.; Nairn, K. M.; Hill, A. J. AGenetically Engineered Protein Responsive to Multiple Stimuli. *Angew. Chem., Int. Ed.* **2011**, *50*, 4428−4431.
(32) Balu, R.; Mata, J. P.; Knott, R.; Elvin, C. M.; Hill, A. J.; Choudhury, N. R.; Dutta, N. K. Effectsof Crowding and Environment on the Evolution of Conformational Ensembles of the Multi-Stimuli-Responsive Intrinsically Disordered Protein, Rec1-Resilin: A Small-Angle Scattering Investigation. *J. Phys. Chem. B* **2016**, *120*, 6490−6503.
(33) Balu, R.; Whittaker, J.; Dutta, N. K.; Elvin, C. M.; Choudhury, N. R. Multi-Responsive Biomaterials and Nanobioconjugates from Resilin-like Protein Polymers. *J. Mater. Chem. B* **2014**, *2*, 5936−5947.
(34) Xia, X. X.; Qian, Z. G.; Ki, C. S.; Park, Y. H.; Kaplan, D. L.; Lee, S. Y. Native-Sized Recombinant Spider Silk Protein Produced in Metabolically Engineered *Escherichia coli* Results in a Strong Fiber. *Proc. Natl. Acad. Sci. U. S. A.* **2010**, *107*, 14059−14063.
(35) Yang, Y. X.; Qian, Z. G.; Zhong, J. J.; Xia, X. X. Hyper-Production of Large Proteins of Spider Dragline Silk MaSp2 by >*Escherichia coli* via Synthetic Biology Approach. *Process Biochem.* **2016**, *51*, 484−490.
(36) Treloar, L. R. G. *The Physics of Rubber Elasticity*; Oxford University Press: New York, 1975.
(37) Aaron, B. B.; Gosline, J. M. Elastinas a Random-Network Elastomer: a Mechanical and Optical Analysis of Single Elastin Fibers. *Biopolymers* **1981**, *20*, 1247−1260.
(38) Pena-Francesch, A.; Jung, H.; Segad, M.; Colby, R. H.; Allen, B. D.; Demirel, M. C. MechanicalProperties of Tandem-Repeat Proteins Are Governed by Network Defects. *ACS Biomater. Sci. Eng.* **2018**, *4*, 884−891.
(39) Kull, S.; Martinelli, I.; Briganti, E.; Losi, P.; Spiller, D.; Tonlorenzi, S.; Soldani, G. Glubran2 Surgical Glue: *in vitro* Evaluation of Adhesive and Mechanical Properties. *J. Surg. Res.* **2009**, *157*, e15−e21.
(40) Wang, H.; Zhang, Q.; Chu, X.; Chen, T.; Ge, J.; Yu, R. GrapheneOxide-Peptide Conjugate as an Intracellular Protease Sensor for Caspase-3 Activation Imaging in Live Cells. *Angew. Chem., Int. Ed.* **2011**, *50*, 7065−7069.
(41) Cobos, M.; González, B.; Fernández, M. J.; Fernández, M. D. Studyon the Effect of Graphene and Glycerol Plasticizer on the Properties of Chitosan-Graphene Nanocomposites via in situ Green Chemical Reduction of Graphene Oxide. *Int. J. Biol. Macromol.* **2018**, *114*, 599−613.
(42) Stepniak, I.; Andrzejewska, E. HighlyConductive Ionic Liquid Based Ternary Polymer Electrolytes Obtained by in situ Photopolymerisation. *Electrochim. Acta* **2009**, *54*, 5660−5665.
(43) Jayathilaka, W. A. D. M.; Qi, K.; Qin, Y.; Chinnappan, A.; Serrano-García, W.; Baskar, C.; Wang, H.; He, J.; Cui, S.; Thomas, S. W.; Ramakrishna, S. Significanceof Nanomaterials in Wearables: A Review on Wearable Actuators and Sensors. *Adv. Mater.* **2019**, *31*, 1805921.
(44) Pan, L.; Chortos, A.; Yu, G.; Wang, Y.; Isaacson, S.; Allen, R.; Shi, Y.; Dauskardt, R.; Bao, Z. AnUltra-sensitive Resistive Pressure Sensor Based on Hollow-sphere Microstructure Induced Elasticity in Conducting Polymer Film. *Nat. Commun.* **2014**, *5*, 3002.

DOI: 10.1021/acs.biomac.9b00389
Biomacromolecules 2019, 20, 3283−3293